N90 17038

COMPARISON OF TWO- AND THREE-DIMENSIONAL NAVIER-STOKES SOLUTIONS WITH NASA EXPERIMENTAL DATA FOR CAST-10 AIRFOIL

R. Charles Swanson, NASA Langley Research Center
Rolf Radespiel, NASA/DFVLR Research Associate
V. Edward McCormick, North Carolina State University

ABSTRACT

The two-dimensional (2-D) and three-dimensional Navier-Stokes equations are solved for flow over a NAE Cast 10 airfoil model. Recently developed finite-volume codes that apply a multistage time stepping scheme in conjunction with steady state acceleration techniques are used to solve the equations. Two-dimensional results are shown for flow conditions uncorrected and corrected for wind tunnel wall interference effects. Predicted surface pressures from 3-D simulations are compared with those from 2-D calculations. The focus of the 3-D computations is the influence of the sidewall boundary layers. Topological features of the 3-D flow fields are indicated. Lift and drag results are compared with experimental measurements.

INTRODUCTION

Wind-tunnel measurements play a key role in the evaluation of aerodynamic prediction techniques. Therefore, accurate determination of the appropriate flow conditions for free air corresponding to a given experiment is necessary. In order to obtain these conditions, procedures are required to provide corrections to the experimental Mach number and angle of attack. The corrections are needed to remove the wind-tunnel-wall interference effects. The range of validity of such correction methods must be defined to indicate when measured data can be used to validate aerodynamic computational schemes.

In the present work, there are three principal objectives related to the problems of aerodynamic computer code validation and wind-tunnel-wall interference. The first objective is to evaluate the capability of a typical wind-tunnel-wall interference correction technique [1] to compute free-air conditions in the case of transonic flow. The second one is to compare numerical solutions with data from a recent experiment with a two-dimensional Cast 10 wing. The final aim is to determine the influence of the sidewall boundary layers in a wind-tunnel flow. These objectives are achieved by solving the two-dimensional (2-D) and three-dimensional (3-D) Navier-Stokes equations. Some recently developed finite-volume codes that apply a multistage time stepping scheme in conjunction with steady-state acceleration techniques are used to solve the equations.

In this paper, pressure and skin-friction distributions from Navier-Stokes solutions are presented for the following conditions:

1. Small supersonic region on upper surface of airfoil.
2. Large supersonic region on upper surface of airfoil.

To emphasize the validity, as well as the breakdown of the computed wall interference corrections, 2-D results are shown for both the uncorrected and corrected flow conditions. The predicted pressures are compared with the experimental data of [2]. Tables I and II summarize the flow conditions considered in this investigation. Points 77 and 81 of [2] are the representative cases. A 2-D solution for Point 78 is also presented.

As indicated in Table II, the representative cases are also computed with a 3-D simulation of the wind-tunnel flow. A comparison is made between the 2-D and 3-D predicted surface pressures. Corrections to the flow conditions due to the upper and lower tunnel walls are used. The focus in the 3-D calculation is the influence of the sidewall boundary layers. Pressure contours and skin-friction lines are displayed to characterize the flow. Topological features of the 3-D flow fields are indicated. Finally, lift and drag predictions are compared with experimental measurements.

TABLE I - Flow Conditions from Experiment of Mineck [2] and for Two-Dimensional Navier-Stokes Calculations

POINT	M_{uncorr}	α_{uncorr}	M_{corr}	α_{corr}	ΔM	$\Delta\alpha$
76	.7658	-1.1769	.7611	-1.3681	- .0047	- .1912
77	.7656	- .3724	.7581	- .6794	- .0075	- .3070
78	.7664	.4887	.7634	.1735	- .0030	- .3152
79	.7661	1.2568	.7540	.7997	- .0121	- .4571
80	.7662	1.6945	.7518	1.1595	- .0144	- .5350
81	.7666	2.1594	.7468	1.5722	- .0198	- .5872

TABLE II - Flow Conditions from Experiment of Mineck [2] and for Three-Dimensional Navier-Stokes Calculations

POINT	M_{uncorr}	α_{uncorr}	M_{corr}	α_{corr}	ΔM	$\Delta\alpha$
77	.7656	- .3724	.7620	- .6540	- .0036	- .2816
81	.7666	2.1594	.7540	1.5810	- .0126	- .5784

MATHEMATICAL FORMULATION

Both the 2-D and 3-D Navier-Stokes equations are considered. The dominant viscous terms for the airfoil and wind-tunnel flows investigated are retained. The viscous transport processes associated with the streamwise direction are neglected. The cross-derivative viscous terms are neglected.

- Mass-averaged Navier-Stokes equations
- Boundary conditions: no slip and adiabatic surface
- Initial solution: free stream
- Constitutive relations
  1) Ideal gas law
  2) Power law for molecular viscosity
- Turbulence closure
  1) Eddy viscosity hypothesis
  2) Algebraic model for viscosity (i.e., Baldwin and Lomax)

NUMERICAL METHOD

In this figure, the basic elements of the present procedures for the numerical solution of the Navier-Stokes equations are given. A modified five-stage Runge-Kutta scheme is used to advance the solution in time. Artificial dissipation terms are added to the difference equations, and they are third order in the smooth region of the flow field. These terms are included for several reasons: (1) to enhance the coupling of the difference equations, (2) to control nonlinear instabilities, and (3) to eliminate oscillations at shock waves.

Three techniques are employed to accelerate convergence to steady state. With local time stepping, the solution at any point in the domain is advanced at the maximum time step allowed by stability. This results in faster signal propagation and, thus, faster convergence. Implicit residual smoothing can be regarded as simply a mathematical step applied after each Runge-Kutta stage to extend the local stability range. Finally, a multigrid method involves the application of a sequence of meshes to a discrete problem to accelerate convergence of the time-stepping scheme. Successively coarser meshes can be generated by starting with the desired fine mesh and eliminating every other mesh line in each coordinate direction. An equivalent fine grid problem is defined on each coarse grid. Appropriate operators are introduced to transfer information between the meshes. There are two main advantages of the multigrid method. First, less computational effort is required on the coarser meshes. Second, information is propagated faster on the coarser meshes due to larger allowable time steps.

Details of the two-dimensional scheme are given in [3]-[5], and the extension to three dimensions is discussed in [6].

- Time integration with 5 stage Runge-Kutta scheme
- Finite-volume spatial discretization -- central differencing
- Second-order accuracy in time and space
- Controlled artificial dissipation -- blending of second and fourth differences
- Acceleration techniques for steady-state solutions
  1) Local time stepping
  2) Implicit residual smoothing
  3) Multigrid

DEFINITION OF MESHES

With a C-type grid, one set of grid lines wraps around the airfoil, and the other set is normal to the airfoil. The normal mesh spacing at the airfoil is 1×10^{-5} chords. For the 3-D case, streamwise planes containing C-type meshes are stacked in the spanwise direction. The distance from the sidewall to the first spanwise point is 2×10^{-5} chords, and approximately 30 grid planes are located within the sidewall boundary layer.

- Two dimensions
  1) C-type grid
  2) 320 streamwise cells (192 on airfoil) , 64 normal cells

- Three dimensions
  1) C-H mesh topology
  2) 256 streamwise cells (192 on airfoil) , 64 normal cells , and 48 spanwise cells

SURFACE PRESSURES FOR CAST 10 AIRFOIL
Point 77

This figure shows a comparison of 2-D Navier-Stokes predictions for the surface pressures with the experimental data of Mineck [2]. Results are given for both the uncorrected and corrected flow conditions. There is better agreement with the data when corrected flow conditions are used.

$Re_\infty = 10^7$

Uncorrected flow conditions

$M_\infty = .766$, $\alpha = -.372$

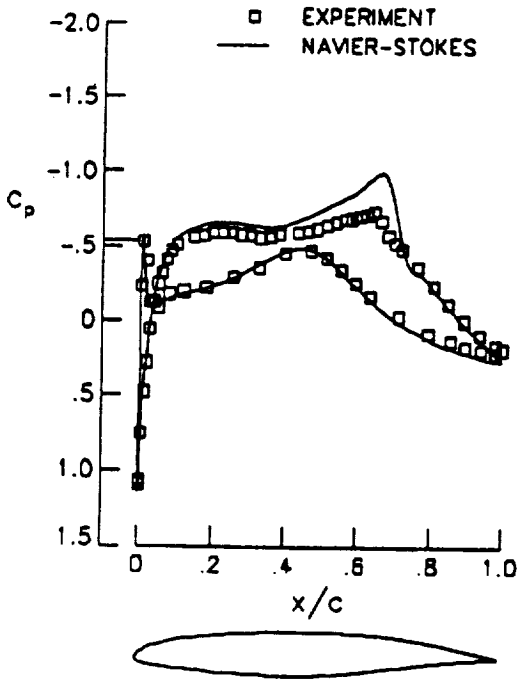

Corrected flow conditions

$M_\infty = .758$, $\alpha = -.679$

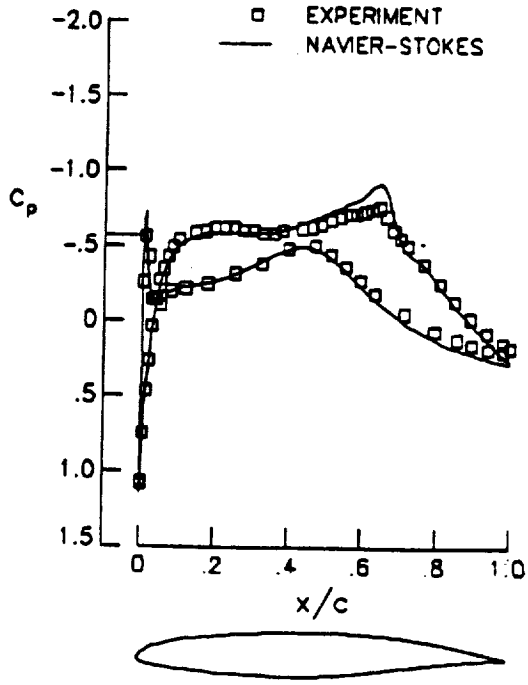

SKIN FRICTION FOR CAST 10 AIRFOIL
Point 77

Calculated skin-friction distributions for the upper surface of the Cast 10 airfoil at both the uncorrected and corrected flow conditions are presented. The decrease in the skin friction at the shock wave is significantly smaller for the case of corrected flow conditions.

UPPER SURFACE , $Re_\infty = 10^7$

Uncorrected flow conditions

$M_\infty = .766$, $\alpha = -.372$

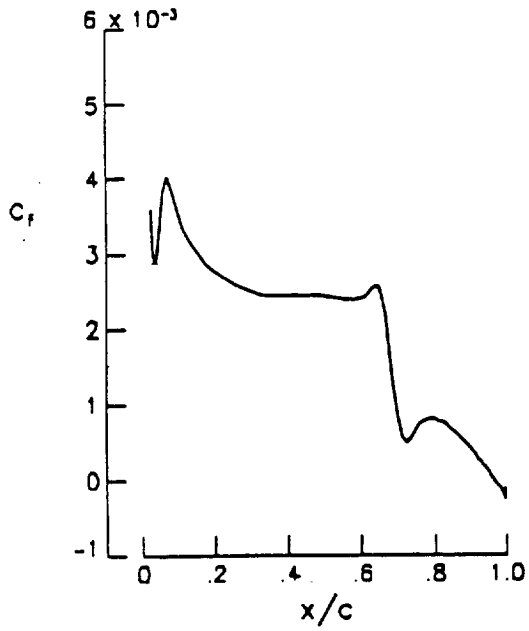

Corrected flow conditions

$M_\infty = .758$, $\alpha = -.679$

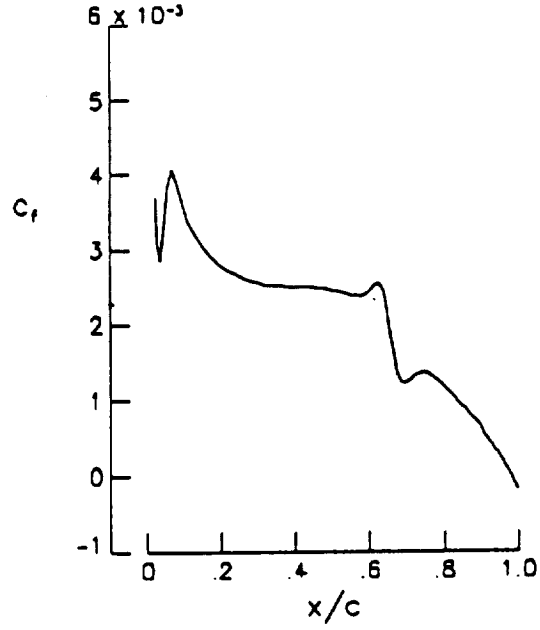

SURFACE PRESSURE FOR CAST 10 AIRFOIL
Point 81

In this figure, computed pressures are compared with experimental data at the uncorrected and corrected flow conditions. There is better agreement with the data when the uncorrected flow conditions are used. The discrepancy between the predicted and measured shock position is probably due to the turbulence model. The corrections for wind-tunnel-wall interference effects are too large. The large supersonic region on the wing results in a behavior of the sidewall boundary layer that is not properly modeled in the wall interference correction code.

$Re_\infty = 10^7$

Uncorrected flow conditions

$M_\infty = .767$, $\alpha = 2.159$

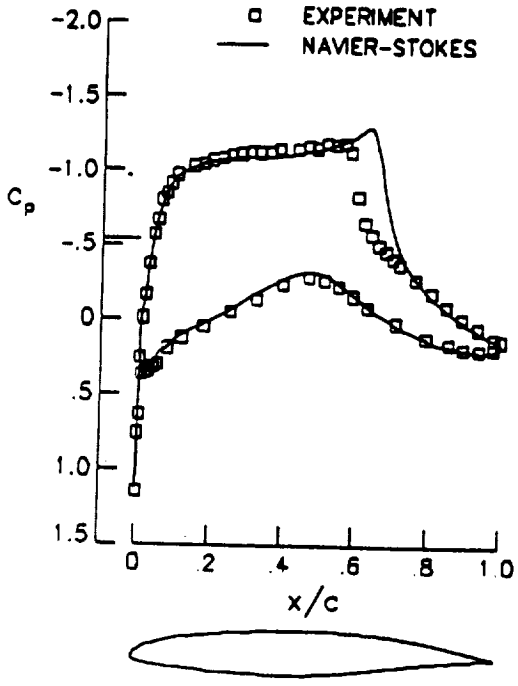

Corrected flow conditions

$M_\infty = .747$, $\alpha = 1.572$

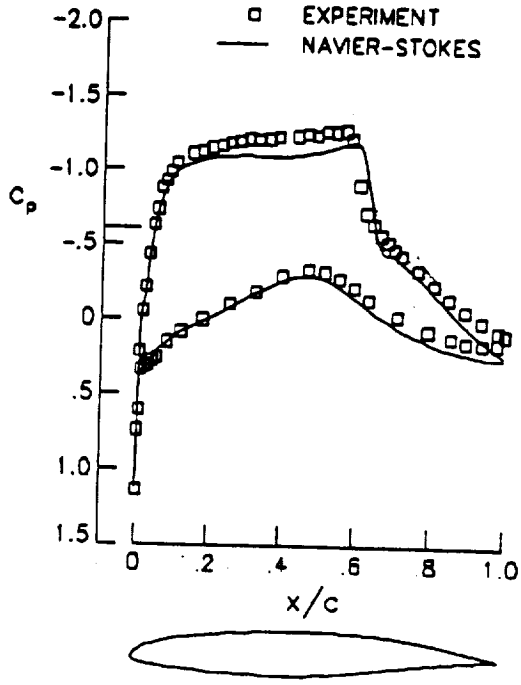

SKIN FRICTION FOR CAST 10 AIRFOIL
Point 81

This figure presents predicted skin-friction variations for the upper surface of the Cast 10 airfoil. The solution based upon corrected flow conditions exhibits a small separation region at the shock and one at the airfoil trailing edge. With the uncorrected conditions, the separation induced by the shock merges with that at the trailing edge.

UPPER SURFACE , $Re_\infty = 10^7$

Uncorrected flow conditions

$M_\infty = .767$, $\alpha = 2.159$

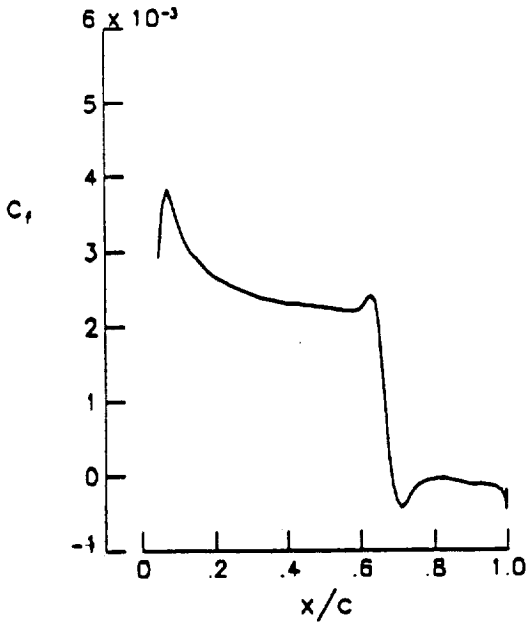

Corrected flow conditions

$M_\infty = .747$, $\alpha = 1.572$

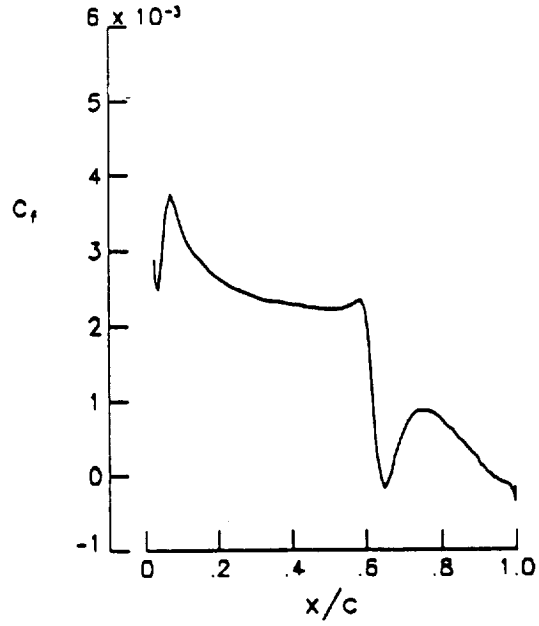

SURFACE PRESSURES FOR CAST 10 AIRFOIL
Point 78

The surface pressure distributions in this figure represent a noticeable departure from those shown previously. They exhibit a weak compression of the upper surface flow followed by acceleration and a shock wave. The computed solution using the corrected Mach number and angle of attack agrees better with the experimental data than the solution using the uncorrected values. However, the weak compression upstream of the shock is still not captured.

$Re_\infty = 10^7$

Uncorrected flow conditions

$M_\infty = .766$, $\alpha = .489$

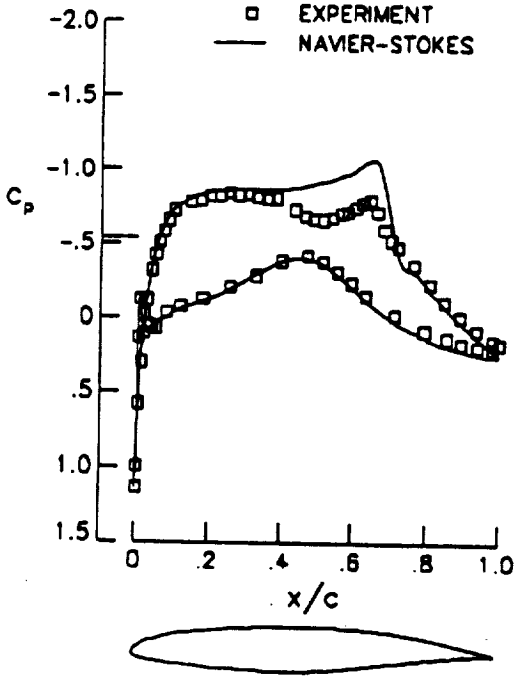

Corrected flow conditions

$M_\infty = .763$, $\alpha = .174$

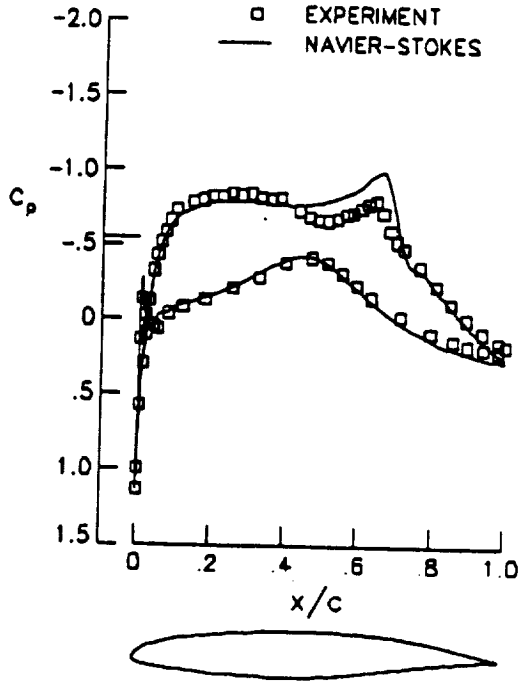

3-D SIMULATION OF CAST 10 AIRFOIL IN WIND TUNNEL

For the 3-D simulation no-slip boundary conditions have been applied on part of the sidewall so that the computed thickness of the sidewall boundary layer matches the values measured in the empty wind tunnel. At the outer boundaries of the computational domain characteristic variable boundary conditions assuming one-dimensional flow normal to the boundary have been employed, and the free-stream conditions are obtained by superimposing the flow field of a single vortex to the onset flow. Due to the displacement effect of the sidewall boundary layer, the Mach number in the test section is not the same as the free-stream Mach number. Therefore, the dependence of the test section Mach number with respect to the free stream was first calibrated by a simulation of the empty wind tunnel. When specifying the flow conditions for the simulations of the airfoil in the tunnel, the wind-tunnel corrections of Mach number and angle of attack for the upper and lower walls as predicted by the method of [1] have been included. Following the ideas of Hung, et al. [7], the turbulence model of Baldwin and Lomax was extended to treat corner flows.

In all simulations, a steady-state solution of the flow has been obtained within 200 multigrid cycles on the fine mesh.

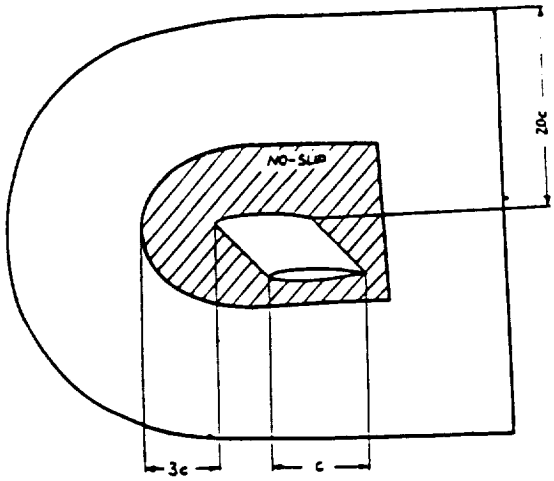

SURFACE PRESSURES FOR CAST 10 AIRFOIL
Point 77

To demonstrate the viscous sidewall effects, results of the 3-D simulation are now compared to those of the 2-D code at the same flow conditions. For $M_\infty = 0.762$, $\alpha = 0.654$, and $Re_\infty = 10^7$, the influence of the viscous sidewall on the pressure distribution along the centerline of the wind tunnel is small.

INFLUENCE OF VISCOUS SIDEWALL

$$M_\infty = .762\ ,\ \alpha = -.654\ ,\ Re_\infty = 10^7$$

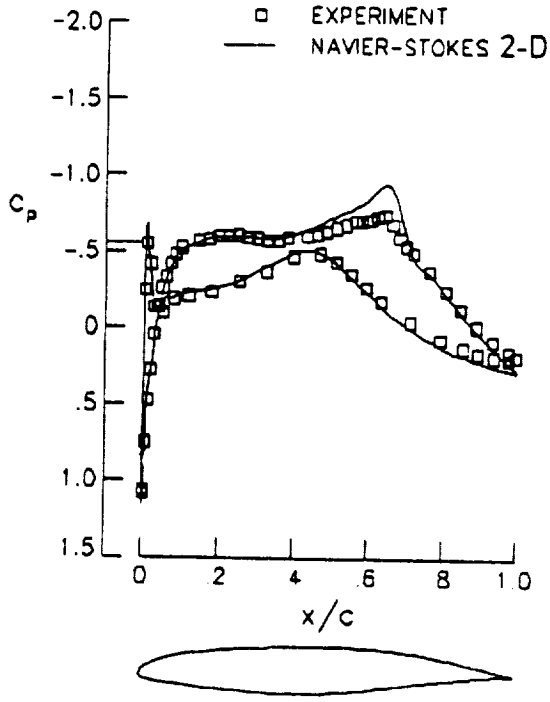

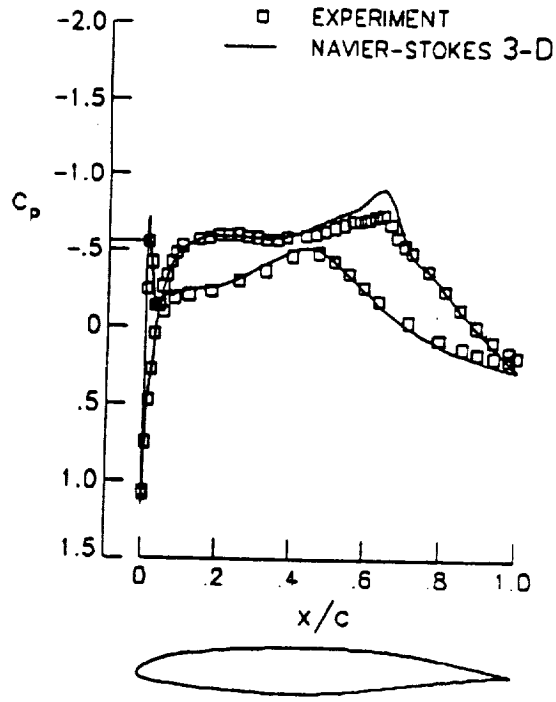

SURFACE PRESSURES FOR CAST 10 AIRFOIL
Point 81

For M_∞ = 0.754, α = 1.581, and Re_∞ = 10^7, the influence of the viscous sidewall on the pressure distribution along the centerline of the wind tunnel is larger. Due to the variation of the displacement thickness of the sidewall boundary layer along the airfoil, the flow is more accelerated at the upper side of the airfoil, and the shock is moved upstream.

INFLUENCE OF VISCOUS SIDEWALL

$M_\infty = .754$, $\alpha = 1.581$, $Re_\infty = 10^7$

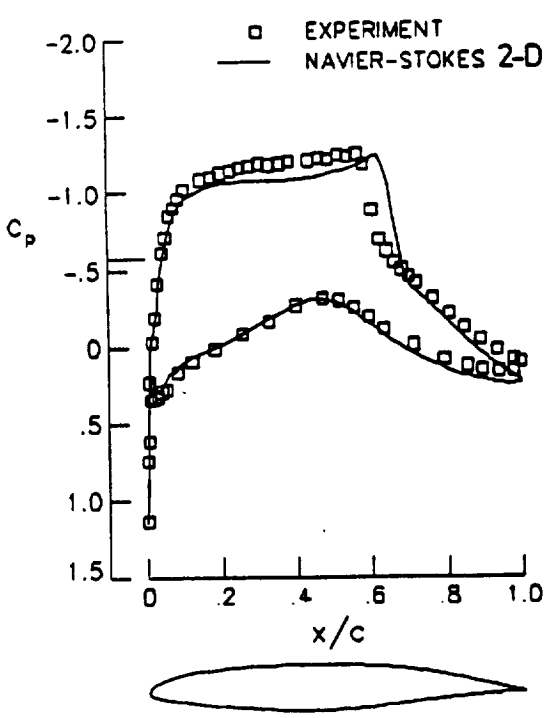

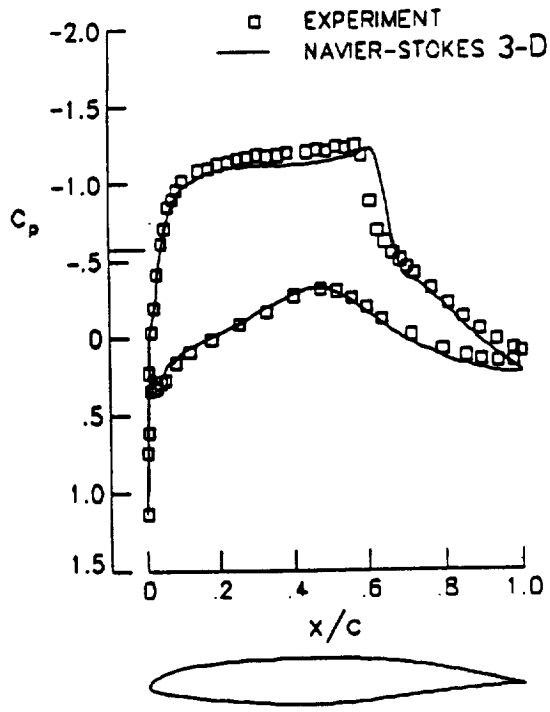

FLOW OVER UPPER SURFACE OF CAST 10 AIRFOIL
Point 77

The pressure contours and the skin-friction lines on the upper surface of the airfoil for $M_\infty = 0.72$, $\alpha = -0.654$, and $Re_\infty = 10^7$ show that the shock is weakened as the sidewall is approached. There is incipient separation at the trailing edge. A small separation around a nodal point occurs in the corner between the trailing edge and the sidewall.

$M_\infty = .762$, $\alpha = -.654$, $Re_\infty = 10^7$

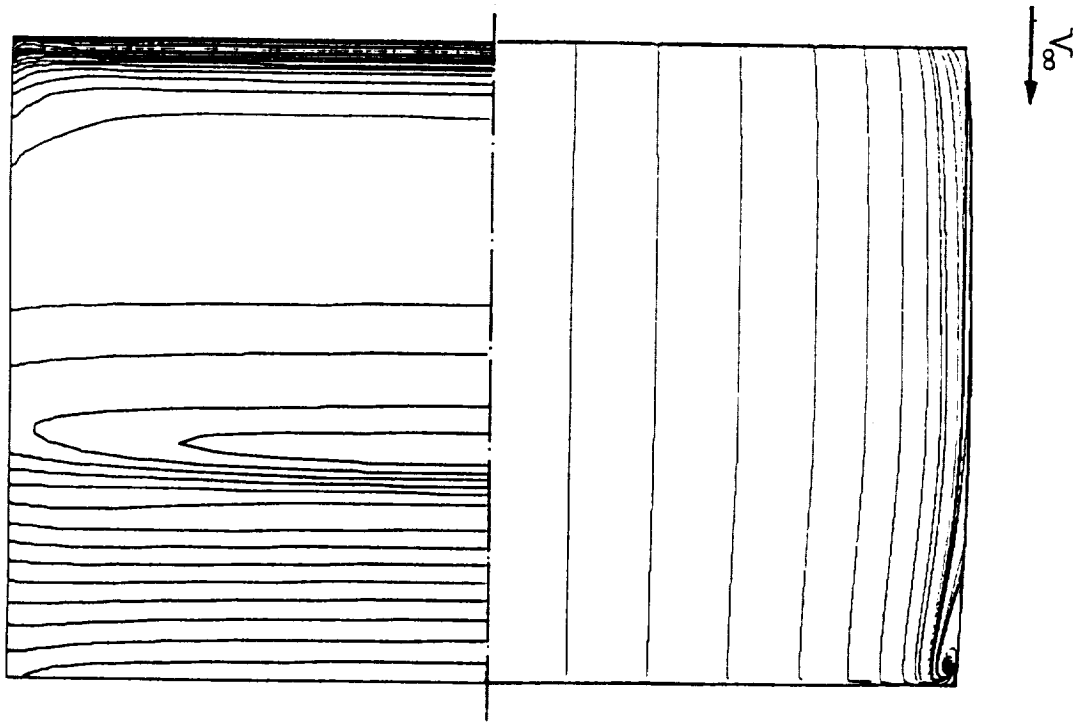

Pressure contours

Skin-friction lines

FLOW OVER UPPER SURFACE OF CAST 10 WING
Point 81

For M_∞ = 0.754, α = 1.581, and $Re_\infty = 10^7$, shock induced and trailing-edge separations occur. These separations are weakened towards the sidewall because the pressure gradients are smaller near the sidewall. The nodal-type separation in the corner between the trailing edge and the sidewall has grown considerably relative to the previous case.

$M_\infty = .754$, $\alpha = 1.581$, $Re_\infty = 10^7$

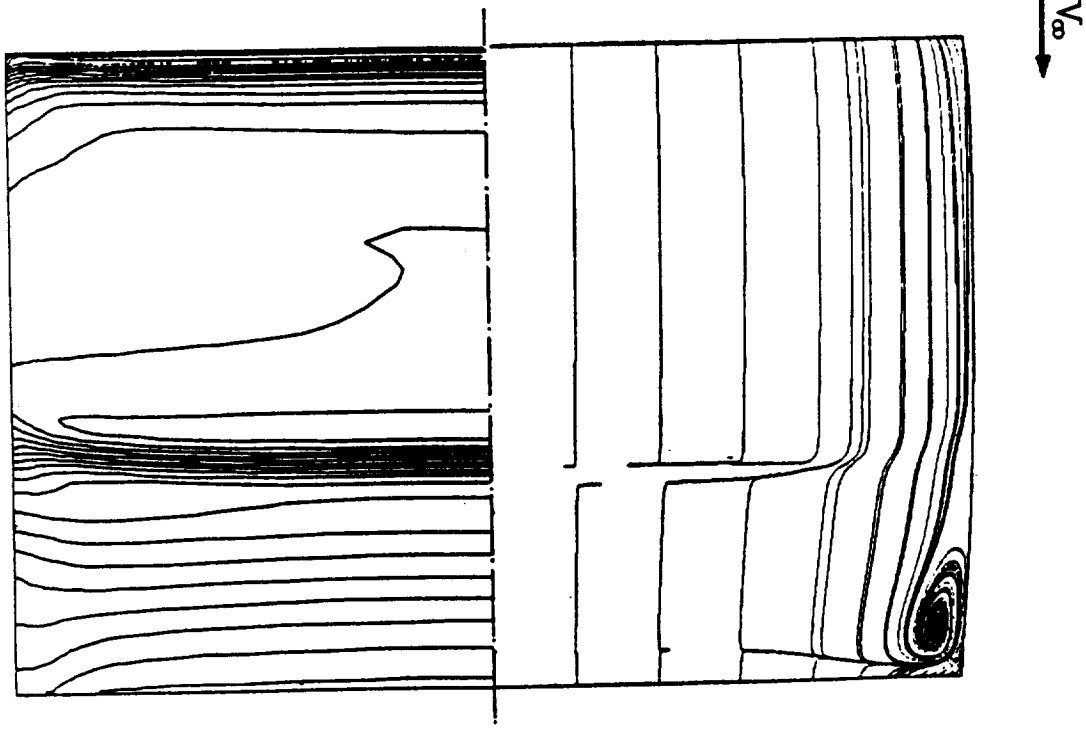

Pressure contours

Skin-friction lines

SKIN-FRICTION LINES FOR WING AND SIDEWALL
Point 77

The skin-friction lines along the wing and sidewall for $M_\infty = 0.762$, $\alpha = -0.654$, and $Re_\infty = 10^7$, show the existence of a sidewall separation upstream of the leading edge of the wing. The wavy behavior of the sidewall streamlines around the trailing edge indicates three-dimensional flow in the corner between the sidewall and the wing.

CAST 10 AIRFOIL , $M_\infty = .762$, $\alpha = -.654$, $Re_\infty = 10^7$

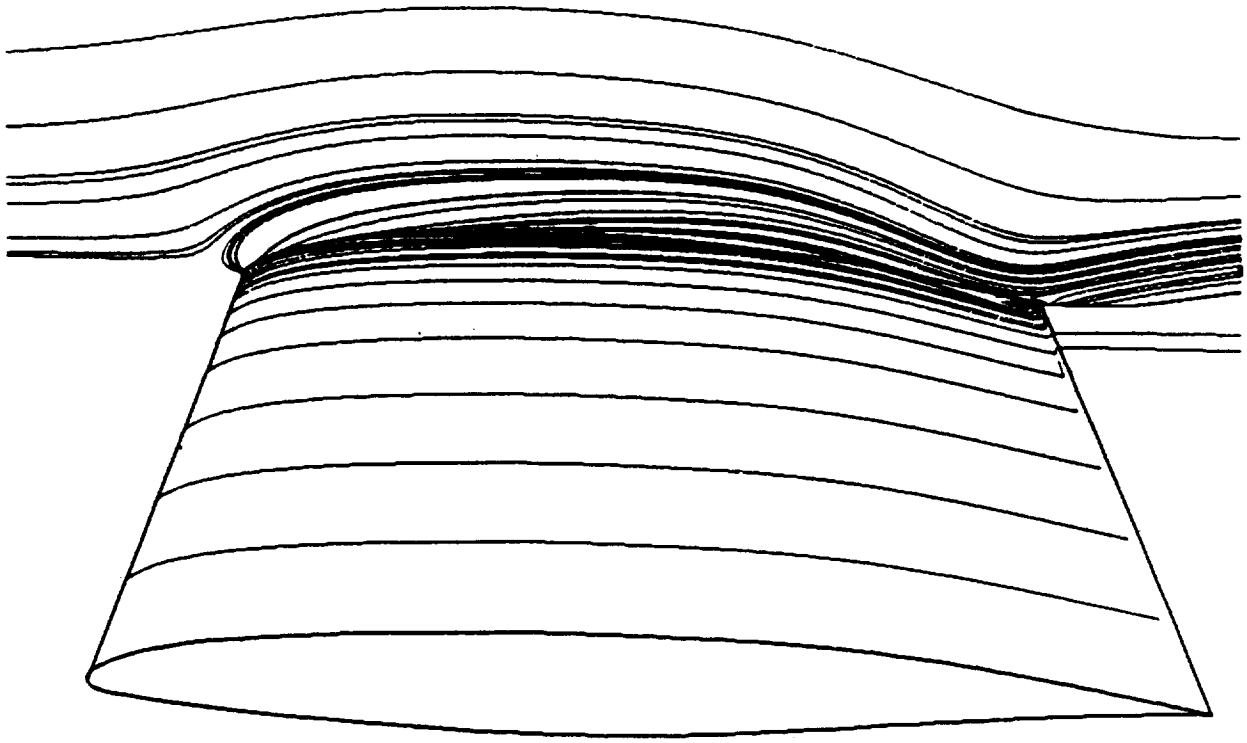

DETAILS OF WING-SIDEWALL JUNCTURE REGION
Point 77

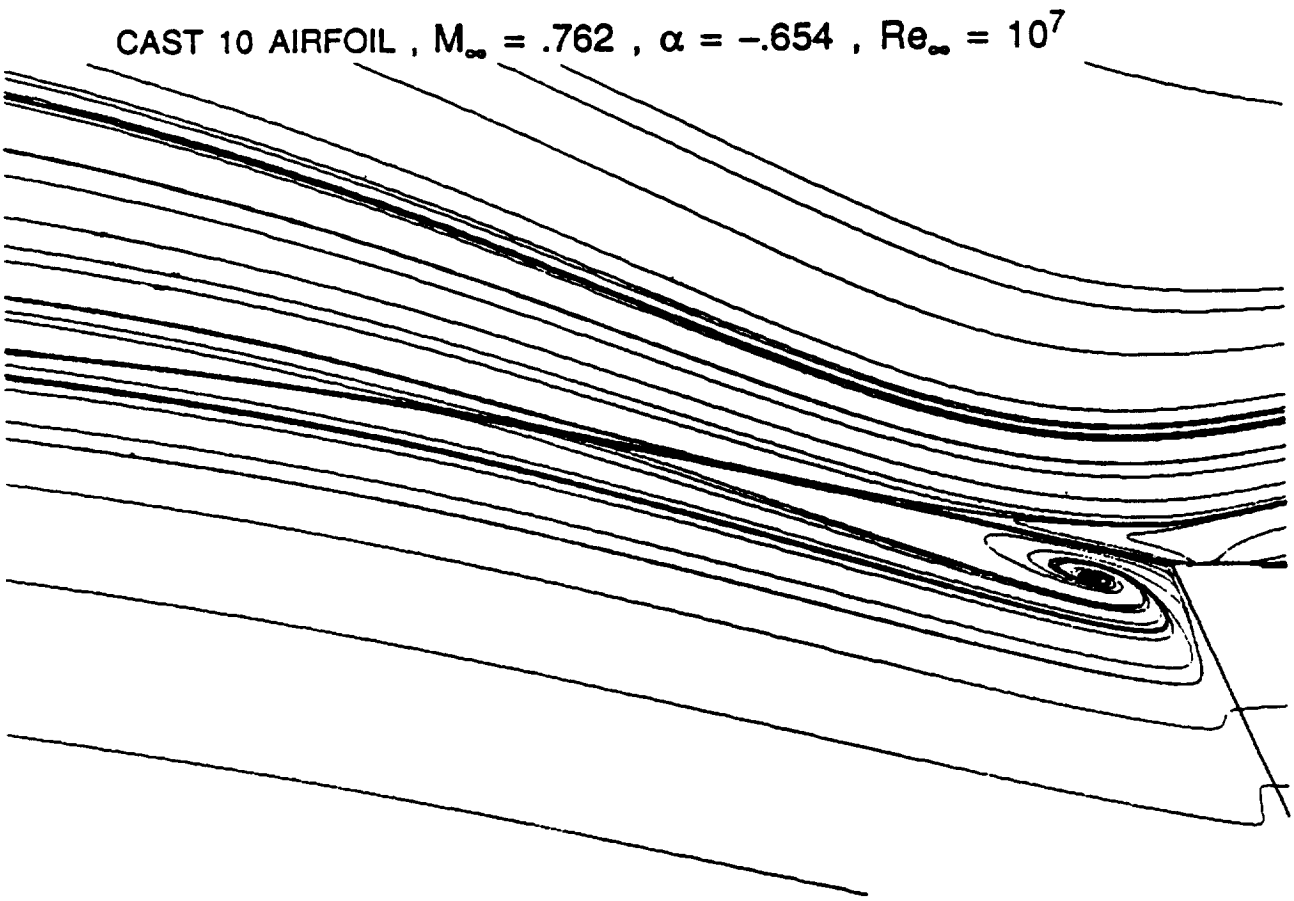

SKIN-FRICTION LINES FOR WING AND SIDEWALL
Point 81

For M_∞ = 0.754, α = 1.581, and Re_∞ 10^7, the sidewall boundary layer separates at the shock and near the trailing edge of the wing, forming a complex flow structure with saddle points and nodal points, which are designated in the figure on the next page by S and N, respectively.

CAST 10 AIRFOIL , M_∞ = .754 , α = 1.581 , Re_∞ = 10^7

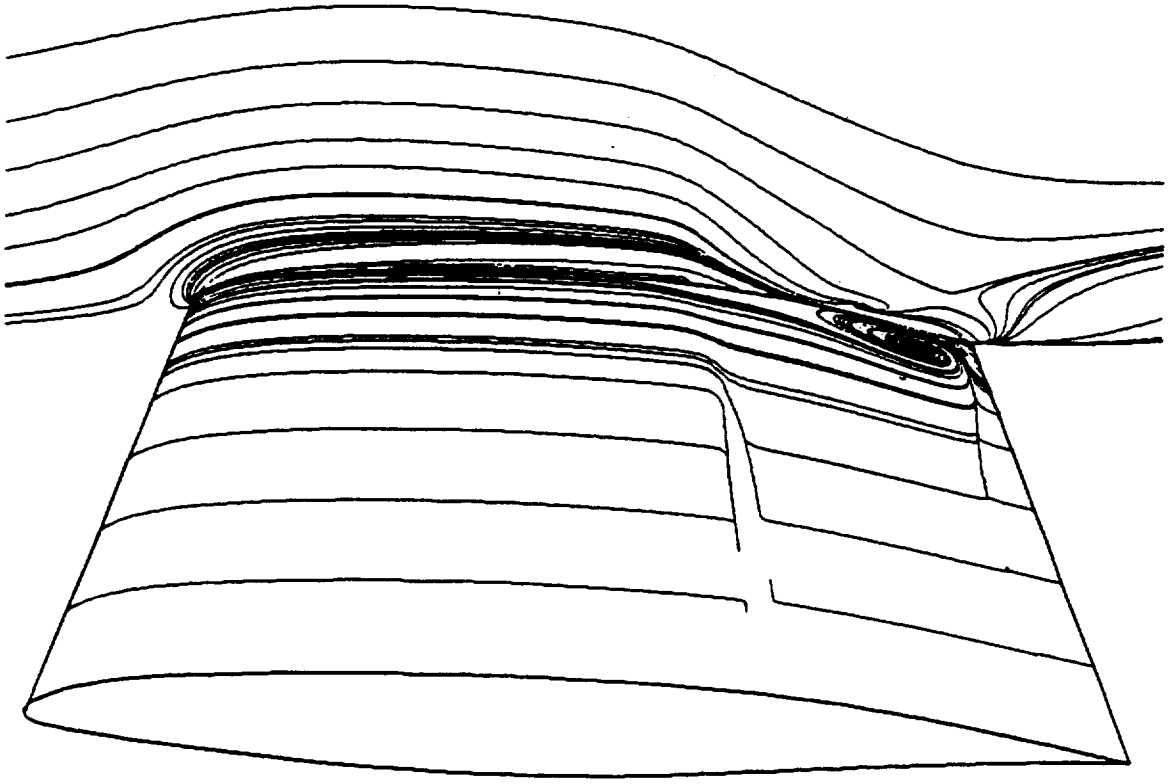

DETAILS OF WING-SIDEWALL JUNCTURE
Point 81

CAST 10 AIRFOIL , $M_\infty = .754$, $\alpha = 1.581$, $Re_\infty = 10^7$

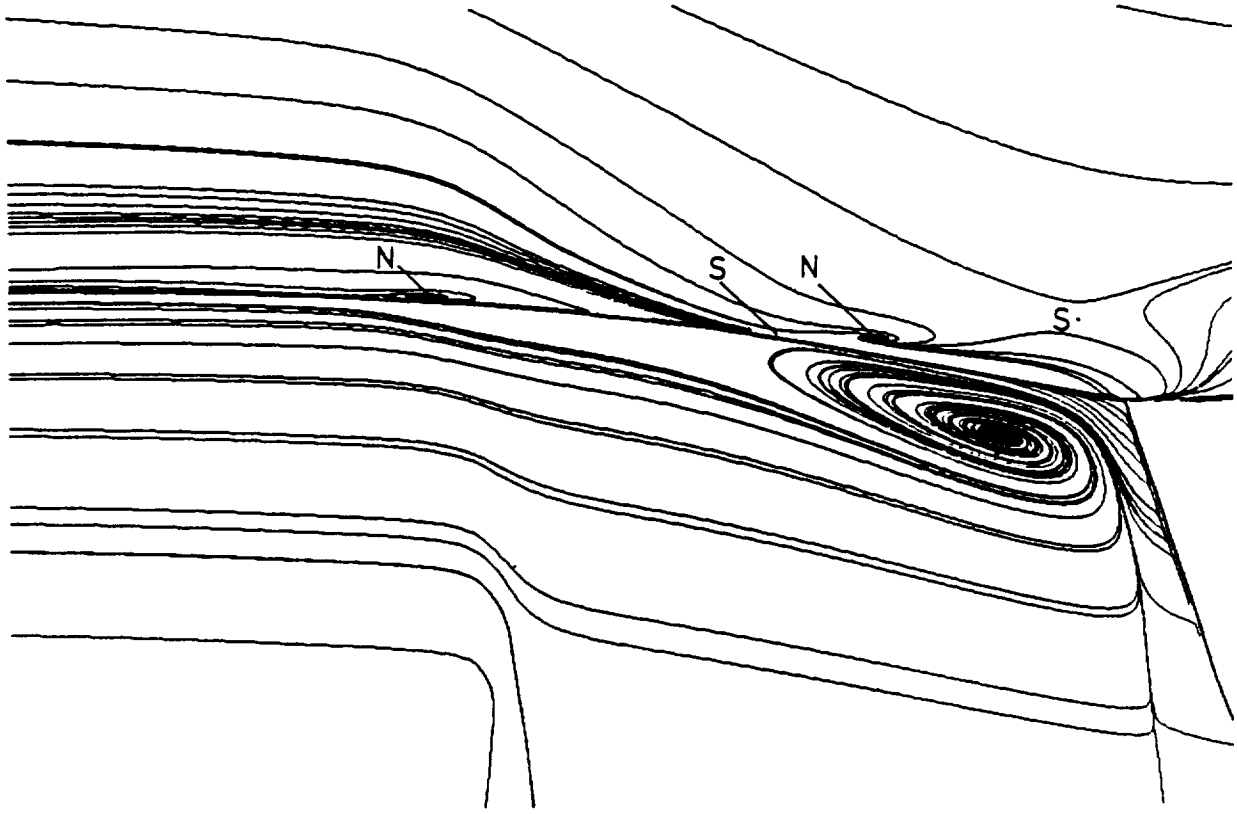

LIFT CURVE FOR CAST 10 AIRFOIL

This figure compares the computed lift curves with the experimental ones for the uncorrected and corrected flow conditions. The predicted lift coefficients are higher than the corrected ones (denoted by square symbol) at the lower angles of attack. As indicated previously, the calculated wall interference corrections are too large at the higher angles of attack, which explains the change in experimental lift curve slope for the corrected conditions. The predicted centerline sectional lift coefficients from the 3-D calculations are indicated with the solid symbol.

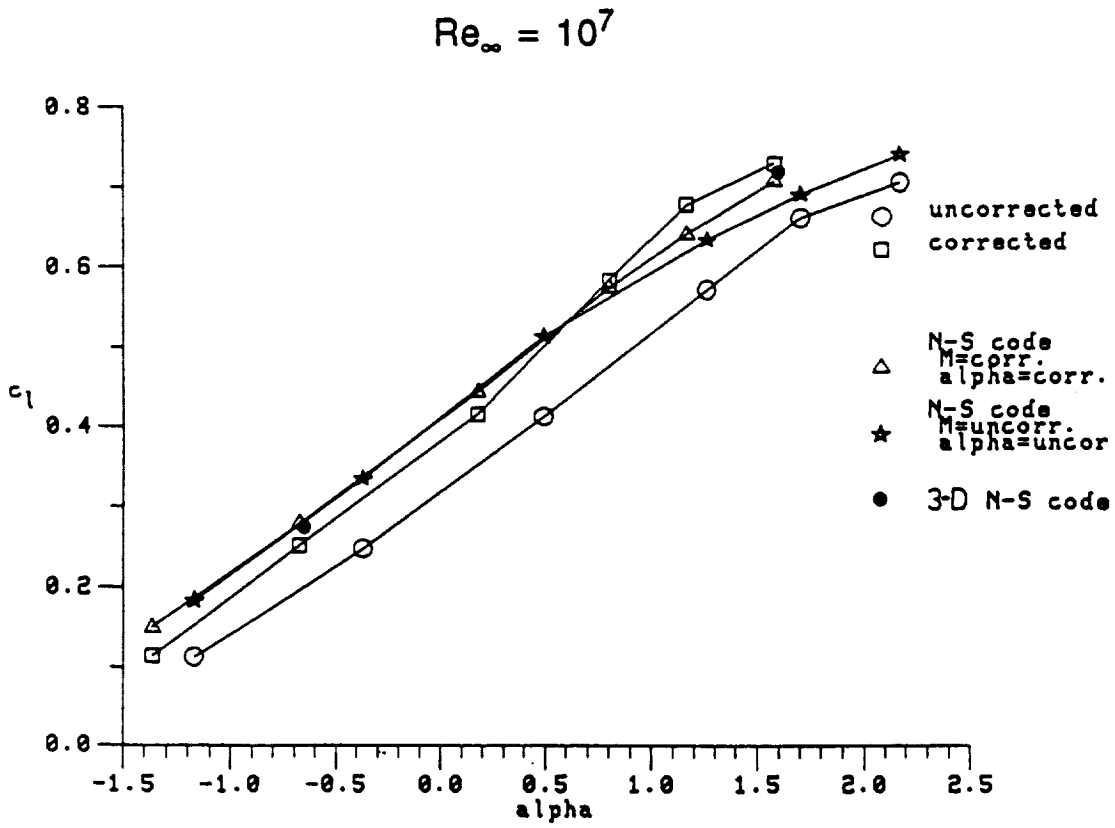

DRAG POLAR FOR CAST 10 AIRFOIL

The computed and experimental drag polars are compared in this figure. There is a strange behavior at the higher angles of attack exhibited by the numerical values based on corrected flow conditions. This occurs because the wind-tunnel-wall interference corrections are too large. The large corrections are a consequence of the breakdown in the theory used to compute the influence of the sidewall boundary layers.

$Re_\infty = 10^7$

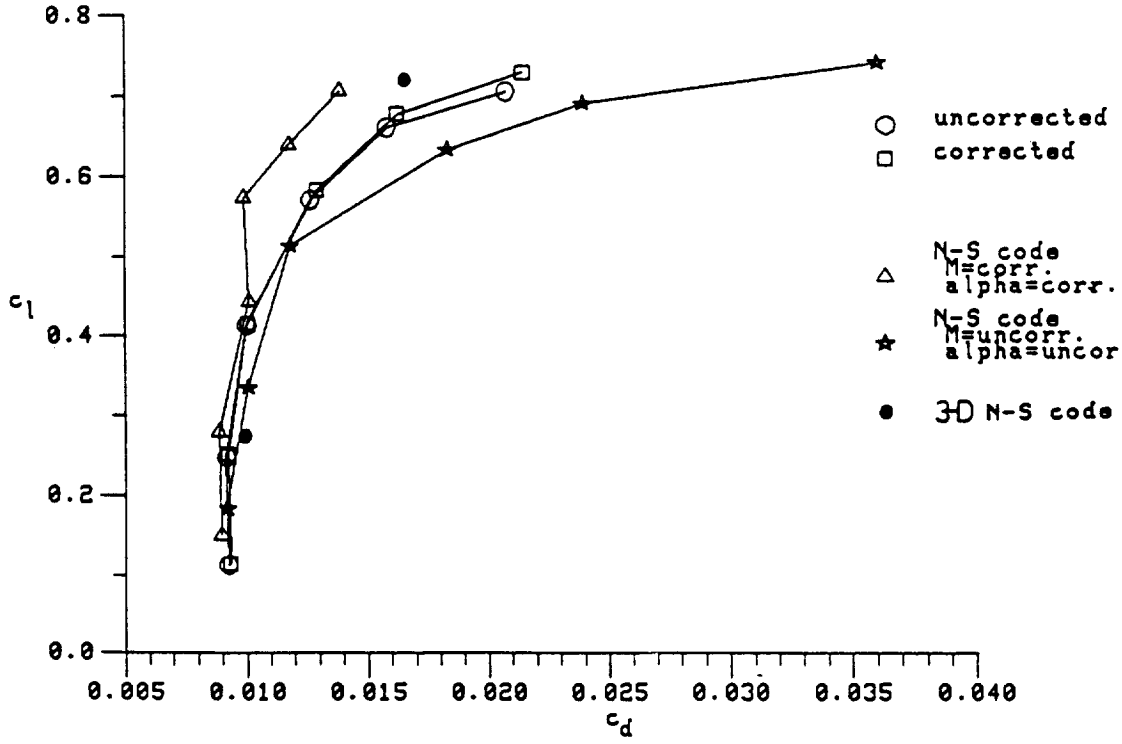

SPANWISE DISTRIBUTION OF DRAG

The spanwise distribution of drag has been computed by integrating pressure drag and friction drag along the airfoil sections. The experimental values have been also included for $M_\infty = 0.762$, $\alpha = -0.654$, and $Re_\infty = 10^7$, whereas for $M_\infty = 0.754$, $\alpha = 1.581°$, and $Re_\infty = 10^7$ there was no experimental drag available [2]. The comparisons show constant drag over 60% of the span and a drag maximum at about 10% of the half span away from the wall. A part of the local increase of the drag may be attributed to the fact that the flow was assumed to be completely turbulent near the sidewall, and boundary-layer transition at 5% of the chord was gradually introduced between 0.25 and 0.35 of the half span. Of course, there is also induced drag to be considered, because the lift is varying over the wing.

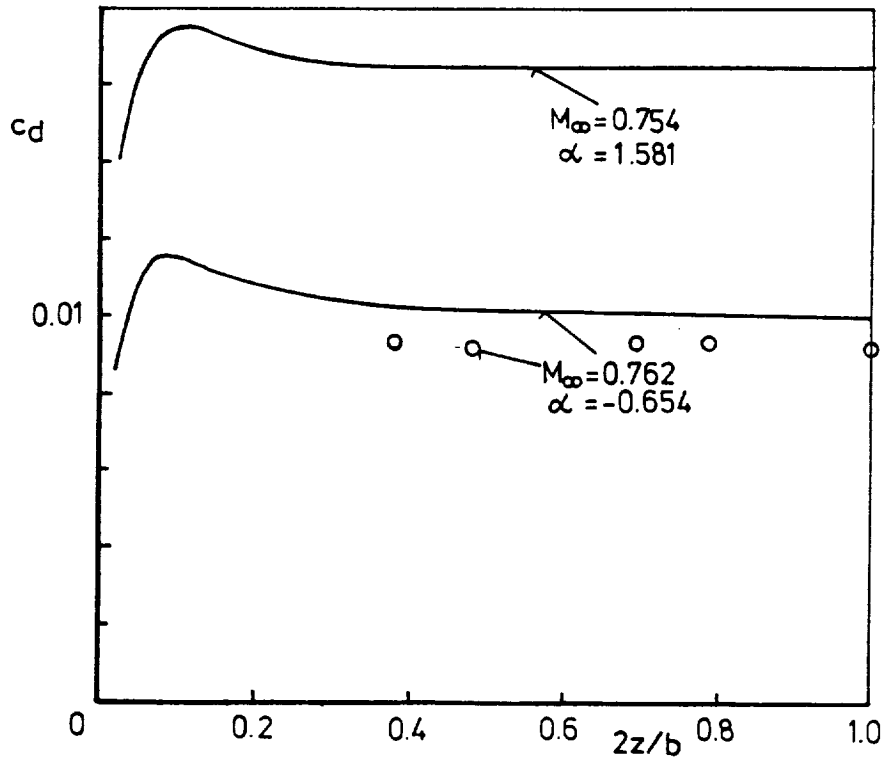

CONCLUDING REMARKS

- Corrections for Mach number and angle of attack due to wind tunnel wall interference effects are required.
- Standard wind tunnel wall interference corrections due to sidewall boundary layers are inadequate in the case of a large supersonic flow region on the upper surface of the wing.
- Three-dimensional simulations of the flow in the wind tunnel have shown that the influence of the sidewall is small for a small supersonic flow region on the wing. For a large supersonic region, the effect of the viscous side wall is to accelerate the flow upstream of the shock and to move the shock upstream.
- For the case of a large supersonic flow region on the upper surface of the wing, the 3-D prediction using only wind tunnel corrections for the upper and lower walls and simulating the sidewall boundary layers is in better agreement with the measured data than the 2-D solution using wind tunnel corrections for all walls.
- For some cases it may be impossible to find wind tunnel corrections such that good agreement is obtained between predictions of 2-D codes and measurements. To address this issue, a 3-D simulation including the upper and lower wind tunnel walls is necessary.
- The Baldwin-Lomax algebraic turbulence model is not adequate to obtain the correct shock wave position for the higher angles of attack considered for Cast-10 airfoil.

REFERENCES

[1] Green, L. L.; and Newman, P. A.: "Transonic Wall Interference Assessment and Corrections for Airfoil Data from the 0.3-m TCT Adaptive Wall Test Section," AIAA Paper 87-1431, 1987.

[2] Mineck, R. E.: "Wall Interference Tests of a CAST 10-2/DoA 2 Airfoil in an Adaptive-Wall Test Section," NASA TM 4015 with Supplement, Dec. 1987.

[3] Arnone, A.; and Swanson, R. C.: "A Navier-Stokes Solver for Cascade Flows," ICASE Report No. 88-32, July 1988.

[4] Radespiel, R.; and Swanson, R. C.: "An Investigation of Cell Centered and Cell Vertex Multigrid Schemes for the Navier-Stokes Equations," AIAA Paper 89-0548, Jan. 1989.

[5] Swanson, R. C.; and Turkel, E.: "Artificial Dissipation and Central Difference Schemes for the Euler and Navier-Stokes Equations," AIAA Paper 87-1107, AIAA 8th Computational Fluid Dynamics Conference, Honolulu, Hawaii, June 9-11, 1987.

[6] Radespiel, R.: "A Cell-Vertex Multigrid Method for the Navier-Stokes Equations," NASA TM, in publication.

[7] Hung, C.-M.; and Buning, P. G.: "Simulation of Blunt-Fin-Induced Shock-Wave and Turbulent Boundary-Layer Interaction," J. F. M. Vol. 154, pp. 163-185 (1985).

☆U.S. GOVERNMENT PRINTING OFFICE:1989-727-067/05005